THE JOURNAL OF PHYSICAL CHEMISTRY A

Article

pubs.acs.org/JPCA

Insights into the Mechanism of an S_N2 Reaction from the Reaction Force and the Reaction Electronic Flux

Santanab Giri,[†,‡,§] Eleonora Echegaray,[†,∥] Paul W. Ayers,[∥] Alvaro S. Nuñez,[‡,§] Fernando Lund,[‡,§] and Alejandro Toro-Labbé*[,†]

[†]Laboratorio de Química Teórica Computacional (QTC), Facultad de Química, Pontificia Universidad Católica de Chile, Casilla 306, Correo 22, Santiago, Chile

[‡]Departamento de Física and [§]CIMAT, Facultad de Ciencias Físicas y Matemáticas Universidad de Chile, Av. Blanco Encalada 2008, Santiago, Chile

[∥]Department of Chemistry, McMaster University, Hamilton, Ontario L8S 4M1, Canada

ABSTRACT: The mechanism of a simple S_N2 reaction, viz; $OH^- + CH_3F = CH_3OH + F^-$ has been studied within the framework of reaction force and reaction electronic flux. We have computationally investigated three different types of reaction mechanisms with two different types of transition states, leading to two different products. The electronic transfer contribution of the reaction electronic flux was found to play a crucial role in this reaction. Natural bond order analysis and dual descriptor provide additional support for elucidating the mechanism of this reaction.

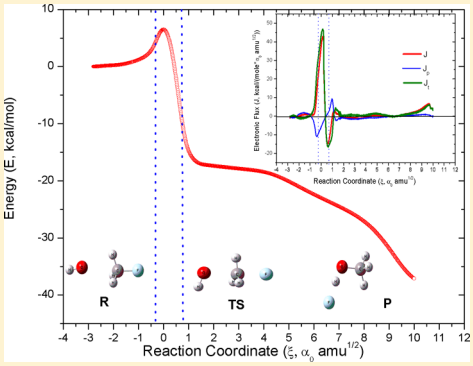

1. INTRODUCTION

One of the most widely studied reactions in organic chemistry is the bimolecular nucleophilic substitution at carbon centers.[1] Extensive theoretical[2−5] and experimental[6−16] studies have been performed to know the exact mechanism of nucleophilic substitution reactions. Nowadays with the help of high level ab initio[14] and density functional theory (DFT)[12,13] calculations, several S_N2 type reactions are fully characterized in terms of energetic and structural parameters. Approaches like Berlin function,[17] electronic stress,[18] second derivative tensor of electron density[19] that have been used to study these reactions each giving results consistent with the reaction force analysis.[20] There are also several chemical dynamics trajectory simulation[21] results, Sun et al.[21] provided valuable information about the S_N2 reaction, $OH^- + CH_3F = CH_3OH + F^-$ by doing both ab initio and direct dynamics classical trajectory simulation calculation. According to them, in most of the cases, the trajectory results lead to the direct dissociated products, thus not following the intrinsic reaction coordinate (IRC) results that lead to an H-bonded complex as product of the reaction.

In this article, we study the gas phase reaction mechanism ($OH^- + CH_3F = CH_3OH + F^-$) using conceptual DFT based reactivity descriptors within the framework provided by the reaction force analysis. To study this type of charge transfer process, conceptual DFT[22−27] provides different types of reactivity descriptors such as the chemical potential[28−30] that measures the escaping tendency of an electron cloud from equilibrium, in analogy to the macroscopic thermodynamics. The newly introduced reaction electronic flux[31,32] (REF), $J(\xi)$, which is the negative of the derivative of the chemical potential along the reaction coordinate, characterizes the electron density rearrangements taking place during the reaction in terms of polarization and net charge transfer contributions. The present article deals with the use of reaction force, reaction electronic flux, and the different components of $J(\xi)$ to get information on specific interactions that drive the reaction. Three reaction paths (I, II, and III) having two different transition states and two different products have been studied. The main emphasis of this article is on the mechanism of the reaction. Section 2 presents the theoretical background for the descriptors that are used to describe the reaction mechanism. Computational details are provided in section 3. Results and discussion are given in section 4.

2. THEORETICAL BACKGROUND

2.1. Reaction Energy and Reaction Force. In any chemical reaction, the reactant is transformed into product through a continuous series of structural changes, which we model via a minimum energy profile ($E(\xi)$) that links the transition state to the reactant and product. The intrinsic reaction coordinate (IRC),[33−37] which is the condensed form

Received: August 2, 2012
Revised: August 31, 2012
Published: September 13, 2012

   dx.doi.org/10.1021/jp3076707 | J. Phys. Chem. A 2012, 116, 10015−10026

of the three-dimensional atomic motion monitors the minimum energy profile of a reaction. The reaction force[20,38,39] is defined as the derivative of $E(\xi)$ with respect to reaction coordinate ξ by the expression

$$F(\xi) = -\frac{dE}{d\xi} \tag{1}$$

For any elementary step of a chemical reaction, the reaction force is characterized by a minimum and a maximum located at ξ_1 and ξ_2. It is already established that, for any single step reaction, there are three reaction regions along ξ: (i) the reactant region ($\xi_R \leq \xi \leq \xi_1$) where the reactants are prepared through structural rearrangements, (ii) the transition state region ($\xi_1 \leq \xi \leq \xi_2$) characterized mainly by electronic reordering, and (iii) the product region ($\xi_2 \leq \xi \leq \xi_P$) where mainly structural relaxation takes place to form the desired product. This feature is very important to characterize different properties along the IRC within the reaction regions.[38−41] In particular, the activation energy ($\Delta E^{\ddagger}$) and the reaction energy (ΔE^0) can be obtained through the analysis of reaction force by the following decomposition:[42−45]

$$\Delta E^{\ddagger} = [E(\xi_{TS}) - E(\xi_R)] = W_1 + W_2 \tag{2}$$

$$\Delta E^0 = [E(\xi_P) - E(\xi_R)] = W_1 + W_2 + W_3 + W_4 \tag{3}$$

where

$$W_1 = -\int_{\xi_R}^{\xi_1} F(\xi)d\xi > 0;\ \ W_2 = -\int_{\xi_1}^{\xi_{TS}} F(\xi)d\xi > 0;$$
$$W_3 = -\int_{\xi_{TS}}^{\xi_2} F(\xi)d\xi < 0;\ \ W_4 = -\int_{\xi_2}^{\xi_P} F(\xi)d\xi < 0 \tag{4}$$

are the reaction works involved in the reaction. The above-defined reaction regions are used to analyze the electronic activity throughout the mechanism of the studied S_N2 reaction. This activity is characterized through a recently developed descriptor property, the reaction electronic flux.[30,31]

2.2. Reaction Electronic Flux. To understand the electronic changes of a system during the course of a chemical reaction, the study of the chemical potential (μ) is the most crucial part because it focuses on the escaping tendency of electrons from an equilibrium distribution. Within the density functional theory framework, for a N electron system having total energy, E, the chemical potential[28−30] has been defined as follows:[29]

$$\mu = \left(\frac{\partial E}{\partial N}\right)_{v(r)} = -\chi \tag{5}$$

Here, $v(\mathbf{r})$ and χ are the external potential and electronegativity, respectively. Applying the finite difference approximation, the chemical potential can be calculated by using ionization potential (IP) and electron affinity (EA) through the following expression:

$$\mu \cong -\left(\frac{IP + EA}{2}\right) \tag{6}$$

In the context of Koopmans' theorem,[46] IP and EA can be approximated with the frontier molecular orbitals energies viz., the highest occupied molecular orbital (HOMO) and the lowest unoccupied molecular orbital (LUMO). Thus, eq 6 can be written in terms of HOMO and LUMO energies, by the expression

$$\mu \cong \left(\frac{E_{LUMO} + E_{HOMO}}{2}\right) \tag{7}$$

where $E_{LUMO} \approx -EA$ and $E_{HOMO} \approx -IP$, as stated by the Koopmans' theorem.[46] The appropriateness of Koopmans' approximation for the electron affinity in Kohn−Sham DFT orbitals is debatable,[47−50] but it suffices for qualitative studies like this one. Thus, eq 7 can be used to approximate the chemical potential at each point of the reaction coordinate, ξ, generating the chemical potential profile $\mu(\xi)$. Corresponding to $\mu(\xi)$, the reaction electronic flux[30,31] is introduced:

$$J(\xi) = -\left(\frac{d\mu}{d\xi}\right) \tag{8}$$

The $J(\xi)$ has been found to be a good descriptor to analyze the behavior of electronic activity during the course of a reaction along the reaction coordinate. It has been observed in previous studies[31,32,51−55] that, when $J(\xi)$ is positive, the electronic activity is driven by bond strengthening or forming processes; similarly, negative $J(\xi)$ implies that the electronic activity is driven by bond weakening or breaking processes. The $J(\xi)$ can also be expressed in terms of electronic polarization $J_p(\xi)$ and electronic transfer $J_t(\xi)$ contributions, which gives valuable information about the change of electronic activity during the course of the reaction:[51−55]

$$J(\xi) = J_p(\xi) + J_t(\xi) \tag{9}$$

The polarization contribution $J_p(\xi)$ can be calculated numerically from a partition of the reactive complex into molecular fragments,[51−55] for an n-fragment system $J_p(\xi)$ is expressed as

$$J_p(\xi) = \sum_{i=1}^{n} J_p^i(\xi) \tag{10}$$

By using the counterpoise method,[56,57] each $J_p^i(\xi)$ can be calculated separately along the intrinsic reaction coordinate, and $J_p^i(\xi)$ can be expressed as follows

$$J_p^i(\xi) = -\left(\frac{N_i}{N}\right)\frac{d\mu_i}{d\xi} \tag{11}$$

where μ_i and N_i are the chemical potential and the number of electrons of fragment i, respectively, and N is the total number of electrons for the supramolecular system.

The flux $J(\xi)$ associated with electronic transfer $J_t(\xi)$ can be obtained from the difference of the total REF, calculated from the supramolecular system, and $J_p(\xi)$:

$$J_t(\xi) = J(\xi) - J_p(\xi) = -\frac{d\mu}{d\xi} + \sum_{i}^{n}\left(\frac{N_i}{N}\right)\frac{d\mu_i}{d\xi} \tag{12}$$

By using the Sanderson's equalization principle for electronegativity,[58,59] which states that the chemical potential is a constant through the system, the chemical potential of the supramolecule (μ) can be written in terms of the chemical potential of hypothetical fragments (μ_i^0) such that $\mu_i^0 \equiv \mu$ for all i, then

$$\mu(\xi) = \sum_{i=1}^{n}\left(\frac{N_i}{N}\right)\mu_i^{\,0}(\xi) \tag{13}$$

dx.doi.org/10.1021/jp3076707 | J. Phys. Chem. A 2012, 116, 10015−10026

Scheme 1. Possible Reaction Mechanism for the S_N2 Reaction $OH^- + CH_3F = CH_3OH + F^-$[a]

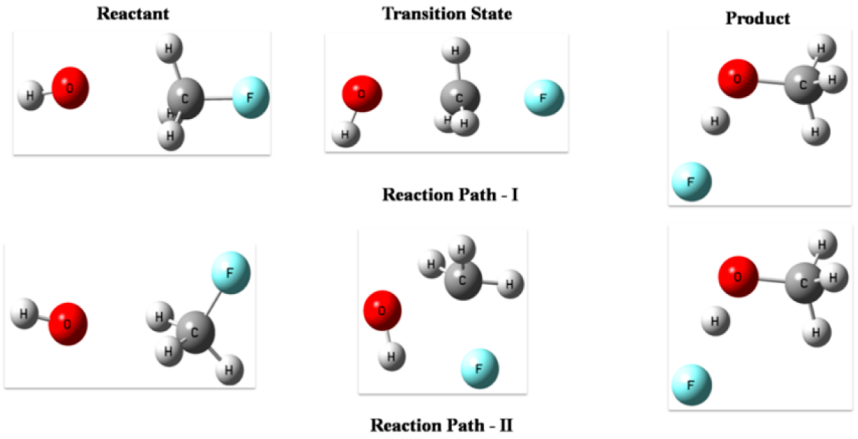

[a]All the structures were optimized at the B3LYP/6-311+G(d) level of theory, and they fulfill their criteria for being reactant, transition state, and product.

and eq 8 can be written as

$$J(\xi) = -\frac{d\mu}{d\xi} = -\sum_{i=1}^{n}\left(\frac{N_i}{N}\right)\frac{d\mu_i^0}{d\xi} \equiv -\sum_{i=1}^{n}\left(\frac{N_i}{N}\right)\frac{d\mu}{d\xi} = \sum_{i=1}^{n} J^i(\xi) \tag{14}$$

From the above discussion on reaction electronic flux, it is observed that, while eq 9 provides a physical (phenomenological) partition of REF through polarization and transfer terms, eqs 11 and 14 give a chemical partition of the reaction electronic flux in terms of the flux contribution from each fragment of the reacting system.

2.3. Fukui Functions and the Dual Descriptor. There are several global and local reactivity descriptors based on conceptual density functional theory to describe the stability, reactivity, and selectivity of a molecule. Among all the local reactivity descriptors, Parr and Yang have introduced the Fukui function[60] ($f(r)$), which is widely used to describe the selectivity inside the molecule. It is defined as the change in electron density $\rho(\mathbf{r})$ with respect to the total number of electrons N at constant external potential,[60] $v(\mathbf{r})$:

$$f(\mathbf{r}) = \left(\frac{\partial\rho(\mathbf{r})}{\partial N}\right)_{v(\mathbf{r})} \tag{16}$$

So that $f(\mathbf{r})$ gives the information about the ability of a molecule to donate (accept) electrons to (from) another molecular system. Using a finite difference approximation two types of Fukui functions[61−65] have been introduced to ascertain the selectivity of a particular center of a system: is the center apt for nucleophilic ($f^+(\mathbf{r})$) or electrophilic ($f^-(\mathbf{r})$) attack? In this context, Morell et al.[66] introduced a new reactivity descriptor, the dual descriptor, that can easily identify the nucleophilic and electrophilic regions of a molecule simultaneously. It can be expressed as

$$\Delta f(\mathbf{r}) \approx [f^+(\mathbf{r}) - f^-(\mathbf{r})] \approx [\rho^{\mathrm{LUMO}}(\mathbf{r}) - \rho^{\mathrm{HOMO}}(\mathbf{r})] \tag{17}$$

where Δf is positive in electrophilic regions and negative in nucleophilic region of a molecule. This dual description has been found to be quite useful and reliable to analyze the reactivity and selectivity inside a molecule.[67−70]

3. COMPUTATIONAL DETAILS

All the geometries have been optimized at Becke, 3 parameters, Lee−Yang−Parr (B3LYP)[71,72] level of theory using 6-311+G(d) basis set. The minimum energy paths from reactant to product via transition state were obtained through intrinsic reaction coordinate (IRC) calculations. Frequencies of reactants, TS, and products were also calculated at the same level of theory. We confirmed that all the transition states possess just one imaginary frequency. Different molecular properties have been calculated using standard methods from single-point calculation at the same level with the geometries obtained from IRC. The counterpoise method is used to determine the fragment's polarization flux by calculating the chemical potential of the individual fragments at each point along the IRC with the geometry they have in the supramolecular system. NBO[73] analysis has also been performed to calculate the Wiberg bond index. The dual descriptor and electrostatic potentials were calculated for reactant, product, and TS to discern the selectivity of the molecular centers along the reaction path. All the calculations were performed using the Gaussian09 suite of programs.[74] To mimic the direct dynamics classical trajectory simulation of the S_N2 reaction, viz., $OH^- + CH_3F = CH_3OH + F^-$, which corresponds to the linear dissociation of the product, we performed a potential energy scan from the transition state geometry at B3LYP/6-311+G(d) level of theory, fixing the angle between O−C−F at 180°, the C−F bond was then gradually increased and decreased to get the desired reactants and products as they appear in the classical trajectory calculations by Sun et al.[21]

4. RESULTS AND DISCUSSION

4.1. Energy Profile and Reaction Force. Three different types of reaction mechanism of a simple S_N2 reaction, viz., $OH^- + CH_3F = CH_3OH + F^-$ have been studied in this work. Scheme 1 depicts a diagram for two possible reaction mechanisms. Two different types of transition state (TS), viz., TSI and TSII, have been found, but the interesting observation is that the products are the same for the two different pathways.

To mimic the reaction path as found by direct dynamics classical trajectory simulation performed by Sun et al., we have also studied the same reaction by fixing the angle between O−

dx.doi.org/10.1021/jp3076707 | J. Phys. Chem. A 2012, 116, 10015−10026

Scheme 2. Possible Reaction Mechanism for the S_N2 Reaction $OH^- + CH_3F = CH_3OH + F^-$ As Found in Direct Dynamics Classical Trajectory Simulation

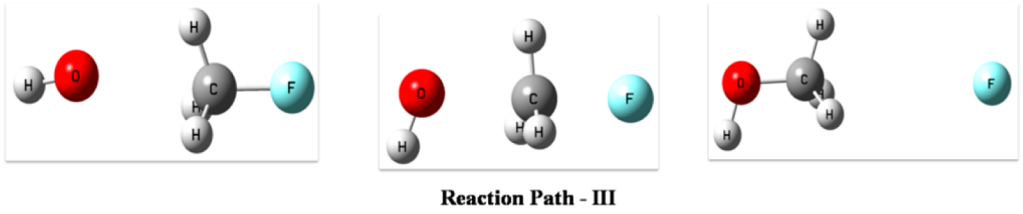

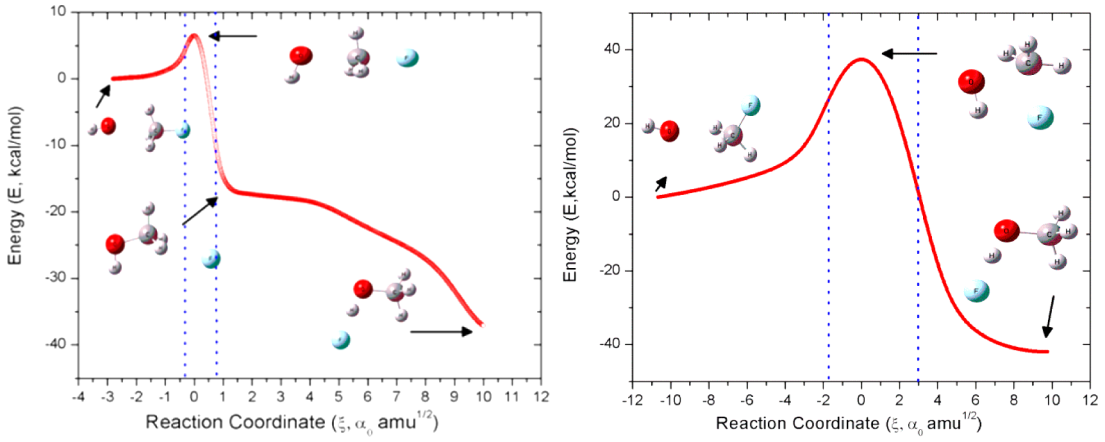

(a) Reaction path – I **(b) Reaction path - II**

Figure 1. Reaction energy profile for a simple S_N2 reaction, viz., $OH^- + CH_3F = CH_3OH + F^-$, in two possible pathways. Vertical lines define the reaction regions obtained from the reaction force analysis.

C–F of the TS and gradually increased and decreased the C–F bond distance to follow the path as shown in Scheme 2.

The minimum energy pathways as found by the intrinsic reaction coordinate calculation are depicted in Figure 1. All the reactions are exothermic in nature due to their negative reaction energy value. In both reaction paths, the products are the same; the only difference is in the orientation of reactants and transition state. The reactant in **path I** is 3.5 kcal/mol more stable than the reactant in **path II**. This difference is due to the change in orientation of OH and CH_3 moieties. While the transition state in **path I** (**TS1**) is perfectly consistent with the chemical S_N2 type, the second transition state (**TS2**) does not follow the expected S_N2 pathway. In reaction **path II** we found a three-membered cyclic TS, which is 20 kcal/mol higher in energy than the **TS1**. From Figure 1, it is apparent that reaction **path I** is more favorable than reaction **path II** as the former possesses a lower activation energy (6.5 kcal/mol) barrier. Although the activation energy difference between the two paths is very large, the reaction energies are very similar (the difference is 10 kcal/mol) because reaction **path I** possess a long IRC to reach the product. In contrast, once the **TS2** is formed, it is very easy to reach the product in the **path II**. To get a more detailed analysis on the different energy barriers, we perform the reaction force analysis.

The corresponding force profile for the two reaction paths is given in Figure 2. According to previous studies, it is clear that the structural rearrangement of reactants to activate the system is dominant in the first step of the activation process. The second step belongs to the reordering of the electronic cloud. From Figure 2a, it is evident that almost 75% of the activation energy corresponds to W_1, which exclusively involves the approach of OH^- toward the C center of CH_3F. The work done in the transition state region, W_2 (ξ_1 to 0), is less than W_1; see the insets of Figure 2. In the case of reaction **path II**, the situation is slightly different (Figure 2b). Here, the work done for the structural rearrangement of reactants (W_1) is 60% toward the activation barrier. The work done in the product region (W_4), which corresponds to the structural relaxation for the two reaction paths, **path I** is almost 10 kcal/mol less than the W_4 for **path II**. If we have a close look at the total work done for two pathways, we found that, for both reaction pathways, structural work predominates. Reaction **path II** has more structural as well as more electronic work than **path I**. In fact, the structural work in **path II** is almost twice that of **path I**. This can be understood by looking at the structure of two transition states. **Path I** possesses a linear TS, so less structural work is needed to reach the TS from the reactant complex; more structural work is necessary to reach the TS in **path II** as it is a three-membered ring structure. From Figure 2a, we can see a long semihorizontal reaction force profile, which is not visible in Figure 2b. This long force profile in **path I** is most probably due to the migration of F^- to form an H-bonded product. We have also found that almost 20 kcal/mol of energy is required for this movement of F^-.

So although the products are similar for the two pathways, **path I** is energetically favorable compared to **path II**. In the next section, we discuss the change in the chemical potential and reaction electronic flux along the reaction coordinate.

4.2. Chemical Potential and Reaction Electronic Flux.

To know the change of electronic activity along the reaction coordinate, we have calculated the chemical potential. This quantity is calculated using eq 7, and the related plots are given in Figure 3. The chemical potential behaves similarly along the reaction coordinate for the two pathways. It remains almost

dx.doi.org/10.1021/jp3076707 | J. Phys. Chem. A 2012, 116, 10015–10026

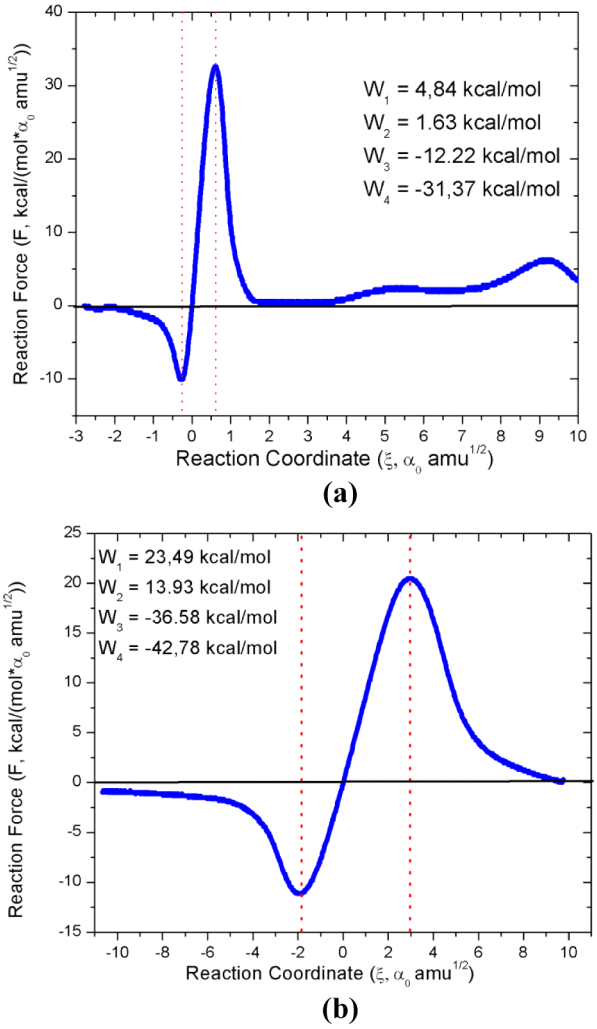

Figure 2. Reaction force profile for a simple S_N2 reaction, viz., $OH^- + CH_3F = CH_3OH + F^-$, in two possible reaction pathways: (a) **path I** and (b) **path II**.

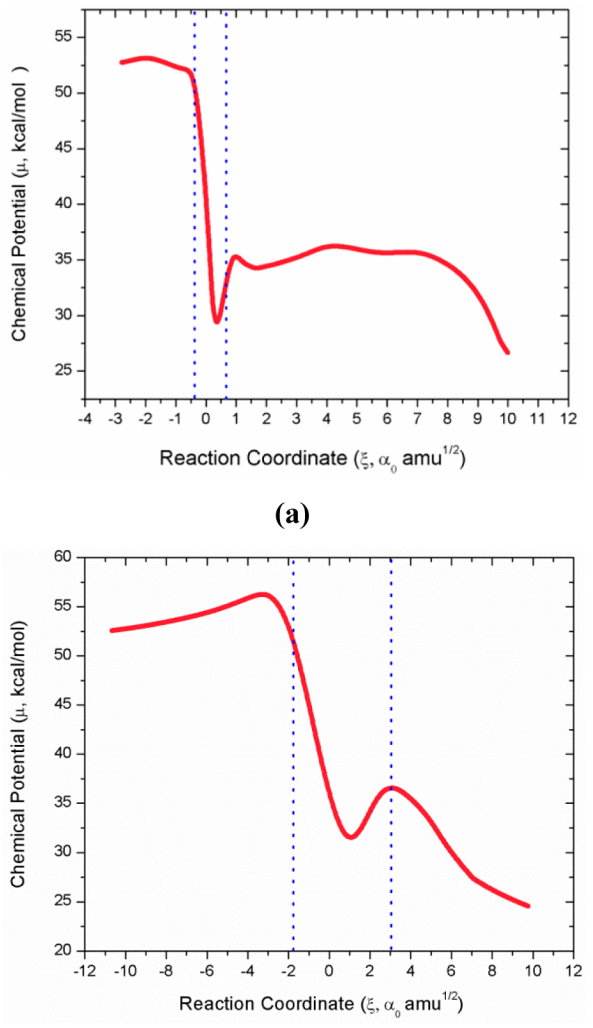

Figure 3. Change of Chemical potential along the reaction coordinate for a simple S_N2 reaction, viz., $OH^- + CH_3F = CH_3OH + F^-$, in two possible pathways: (a) **path I** and (b) **path II**.

constant within the reactant region, the maximum change is observed in the transition state region. In this region, the chemical potential decreases up to the transition state structure; then, it increases until the end of the transition state region. In the product region, it again decreases. To explore, in depth, the electronic activity that takes place along the intrinsic reaction coordinate, the reaction electronic flux (REF) has been calculated using eq 8.

Figure 4 tells about the change in REF along the IRC for the two different pathways. The zero flux regimes in the reactant region for both the pathways imply that the OH^- approaches the C center, determining the first part of the activation energy W_1. In this region, structural arrangements take place to initiate the reaction. After this, the electronic activity starts with the O−C bond formation and weakening of the C−F bond. The REF is more intense in **path I** (Figure 4a) than in **path II** (Figure 4b). The positive flux in the TS region implies that the spontaneous electronic activity associated to the bond making process drives the electronic activity in this part of the reaction. If we take a look at the IRC for both reaction paths, we find that, up to the TS region, the profile looks similar, but the profile in the product region is different. We found a small positive peak for **path I** after a long zero flux regime, whereas it is visible for **path II** right after the flux profile enters to the product region. The zero flux profile in the product region for **path I** implies that structural relaxation is predominant. This is, we found a local minimum that corresponds to a structure in which C−O bond is being formed and F is away from the **CH_3OH** moiety in the energy profile. Further, when the IRC went on, we found again a small positive flux (Figure 4a). This is most probably due to the formation of the hydrogen-bonded complex; although in the product region, structural relaxation is predominant, but the detached **F** moiety still has some electronic activity. This electronic activity helps the **F** moiety to come again close to the **H** of **OH** moiety to form a stable H-bonded complex. For **path II**, the situation is quite straightforward. In this case, we observed a broad positive flux region in the product region (Figure 4b). We did not see any zero flux regime in the product region as no local minimum was found in the IRC calculation. The explanation for positive flux in the product region for **path II** is the same as we discussed previously for **path I**.

To explain this, we also performed the separation of reaction electronic flux, $J(\xi)$ into two fluxes viz., electronic polarization, $J_p(\xi)$, and electronic transfer contribution, $J_t(\xi)$, by doing the

dx.doi.org/10.1021/jp3076707 | J. Phys. Chem. A 2012, 116, 10015−10026

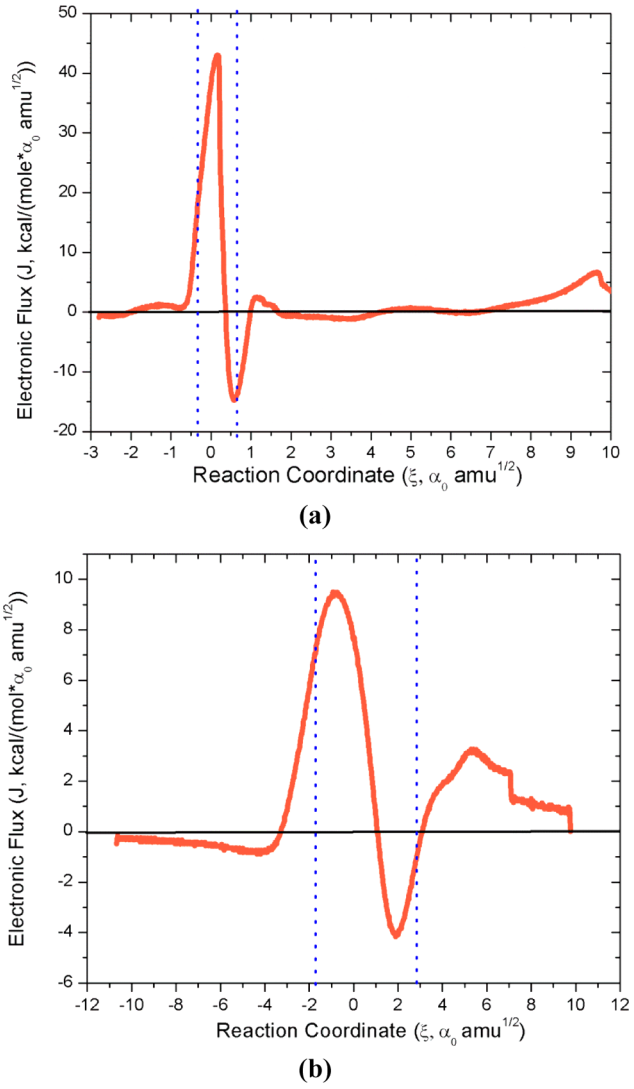

Figure 4. Reaction electronic flux profile for a simple S_N2 reaction, viz., $OH^- + CH_3F = CH_3OH + F^-$, in two possible reaction pathways along the reaction coordinate: (a) **path I** and (b) **path II**.

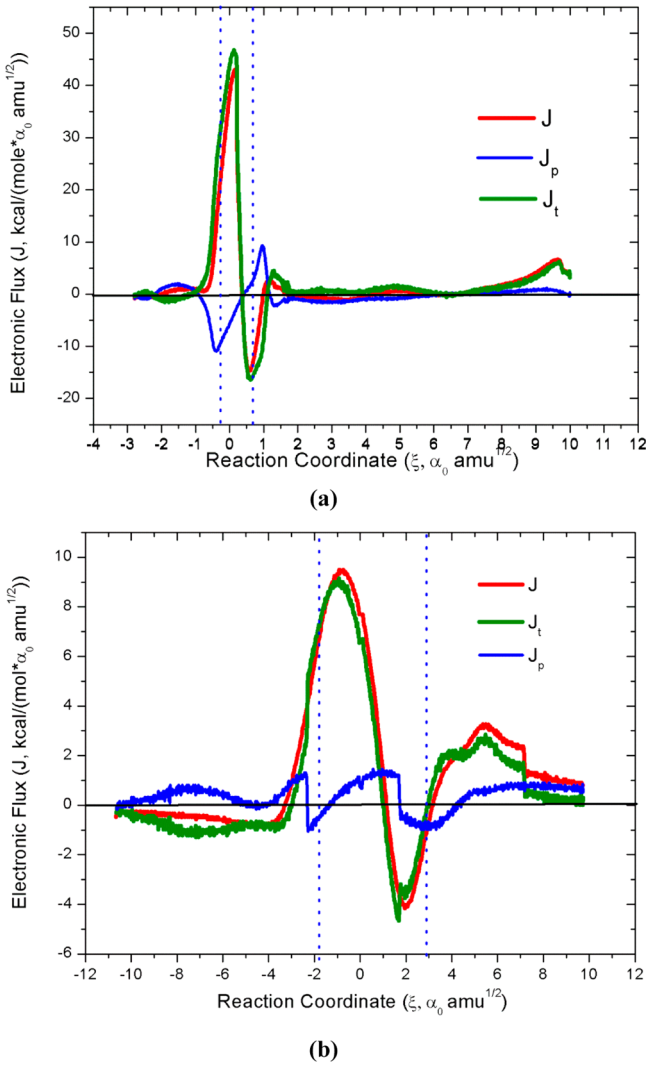

Figure 5. Reaction electronic flux separation profile for a simple S_N2 reaction, viz., $OH^- + CH_3F = CH_3OH + F^-$, in two possible reaction pathways along the reaction coordinate: (a) **path I** and (b) **path II**.

counterpoise calculation on different fragments of the $[OH\cdots CH_3\cdots F]$ moiety. The result is shown in Figure 5.

From Figure 5, it is evident that the electronic transfer contribution of the electronic flux is the most important feature throughout the reaction. The contribution from polarization $J_p(\xi)$ is only evident in the transition state regions. The transition state regions for both pathways have major electronic transfer contributions $J_t(\xi)$. This implies that, in the transition state region, the electronic transfer occurs from **OH** to **C** to **F** center and that electronic transfer is the driving force of the reaction. Now, we look at the individual fragment contribution to the electronic transfer and electronic polarization flux to characterize the response of the fragments during the reaction. The related plots are given in Figures 6 and 7. Figure 6 illustrates the electronic transfer contribution of individual fragments for two different reaction pathways.

From Figure 6, it is evident that, for both reactions, the trends featured by the electronic transfer flux are quite similar, for all three individual moieties in three reaction regions. However, there is a slight difference in the transition state region. For both reaction paths, the contribution of electronic transfer for the CH_3 moiety is less than the other two moieties, **F** and **OH**. If we have a close look at the transition state region, we see that the contribution of electronic transfer is greatest for **OH** until the reaction reaches the transition state. After that, it is the **F** moiety whose contribution is more important than those of the **OH** and CH_3 moieties. This situation is different when we look at the electronic polarization contribution, as depicted in Figure 7.

In **path I**, we found that, in the transition state region, the electronic polarization contribution for CH_3 is more significant than for the other two moieties, but the pattern is different in the reactant and product regions. We found that, in the reactant region, the main contribution comes from **OH**. In the product region, **F** is the main contributor to the electronic polarization flux. So, from the above explanation, we can say that, while **OH** and **F** are the two most crucial moieties throughout the reaction paths, CH_3 plays an important role in the transition state region. This can be explained nicely if we have a look at the transition state structure of **path I**. Here **F**, CH_3, and **OH** moieties exist in a linear geometry, so the electronegative **F** and **OH** makes the CH_3 highly polarizable. In the reactant complex, there is a bond between **C−F**, and **OH** is away from CH_3, so

dx.doi.org/10.1021/jp3076707 | J. Phys. Chem. A 2012, 116, 10015−10026

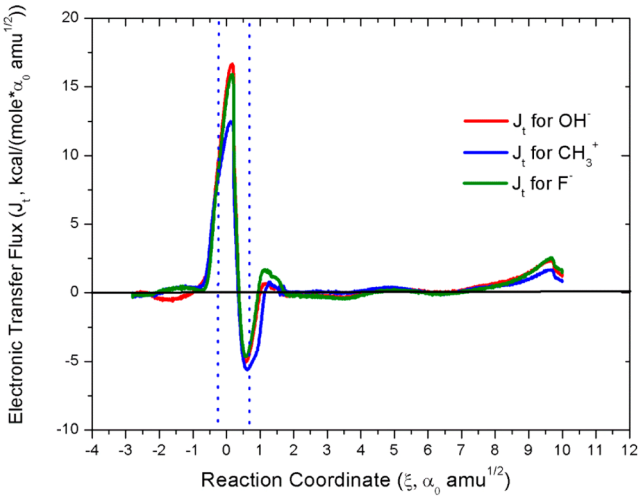

(a)

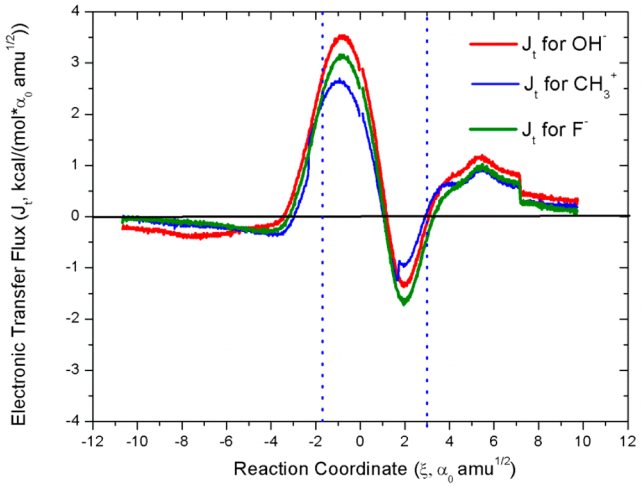

(b)

Figure 6. Electronic transfer flux profile for individual component of a simple S_N2 reaction, viz., $OH^- + CH_3F = CH_3OH + F^-$, in two possible reaction pathways along the reaction coordinate: (a) **path I** and (b) **path II**.

the polarization flux of **CH_3** is less. As **F** comes out from **CH_3** during the formation of **TS**, it has an impact on **CH_3** resulting in the negative polarization flux profile (Figure 7). After this, the flux starts increasing due to the approaching **OH** moiety toward **CH_3** to form a bond between C−O. The flux reaches the maximum when the C−O bond is formed. So in **path I**, there is a clear impact of **F** and **OH** toward the polarization flux of **CH_3**. This has not been observed in **path II** as here **TS** is not linear, it is cyclic. We did not find any prominent **CH_3** polarization flux in the TS region (not shown here). In fact, we found that, throughout the reaction, there are no significant electronic polarization contributions from all three components in **path II**.

4.3. Natural Bond Order Analysis. To look for consistency with the above observations, it is very important to know which bonds are breaking or forming during the course of the reaction. To serve this purpose, we have calculated the Wiberg index along the intrinsic reaction coordinate. The evolution of Wiberg bond order and its derivative along the IRC are displayed in Figures 8 and 9,

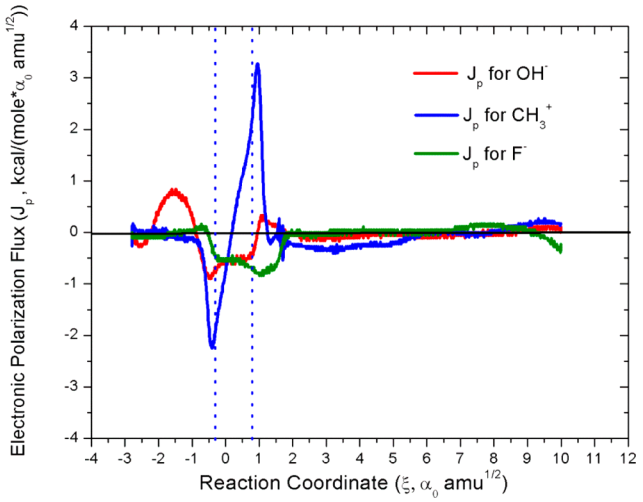

Figure 7. Electronic polarization flux profile for an individual component of a simple S_N2 reaction, viz., $OH^- + CH_3F = CH_3OH + F^-$, in **path I** along the reaction coordinate.

respectively. It is observed from Figure 8 that, for both reaction paths, O−C bond is forming and that, simultaneously, C−F bond is breaking along the reaction coordinate. If we look at the beginning of the reaction, we see that the bond order of O−C and C−F are roughly 0.1 and 0.8. This indicates that, in the reactant, there is a bond between C−F and no bond between C−O. In the TS region, the bond order of C−F decreases from 0.8 to about 0.5, and the C−O bond order increases from 0.1 to about 0.5. This indicates that the C−F bond is about to break and that the C−O bond is about to form. At the end of the reaction, the bond order of O−C and C−F are roughly 1.0 and 0.0, indicating that, in the product, the O−C bond is being formed and that there is no bond between C−F. This phenomenon is more visible when we look at the derivative of the Wiberg index depicted in Figure 9. It is clear from the Figures 8 and 9 that the bond making and breaking takes place simultaneously along the reaction path and that the maximum change occurs in the transition state region. This analysis also supports the view that the electronic transfer contribution of the reaction electronic flux associated with bond formation and breaking is predominant throughout the reaction. During the course of the reaction, electronic rearrangements occur, resulting in the formation of the C−O bond and weakening of the C−F bond.

4.4. Dual Descriptor. In the S_N2 reaction, the nucleophile attacks the electrophilic center from the back, so it is important to know which part of the reactant acts as nucleophile, or electrophile, during the course of the reaction. For that purpose, we have calculated the dual descriptor at six key points in **path I** and four points in **path II** along the reaction force profile. Figures 10 and 11 display the corresponding dual descriptor of reactant, force minimum and force maximum, and the product for reaction **paths I** and **II**, respectively. Areas in blue are nucleophilic sites having $\Delta f(\mathbf{r}) < 0$; areas in red are electrophilic site having $\Delta f(r) > 0$. From Figures 10 and 11, it is evident that the reactant and the product have the same type of reactivity. OH^- acts as a nucleophile and CH_3 as an electrophilic center in both cases, but a difference in the reactivity pattern of the transition state is observed. In the transition state for **path I**, the OH^- still has nucleophilic character, but for **path II**, both OH^- and F^- have nucleophilic

dx.doi.org/10.1021/jp3076707 | J. Phys. Chem. A 2012, 116, 10015−10026

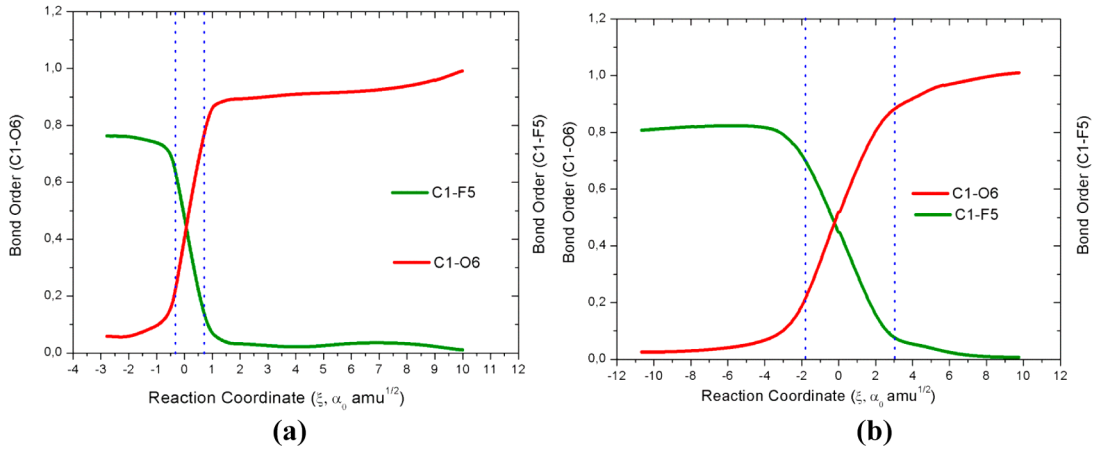

Figure 8. Wiberg bond order evolution of a simple S_N2 reaction, viz., $OH^- + CH_3F = CH_3OH + F^-$, in two possible reaction pathways along the reaction coordinate: (a) **path I** and (b) **path II**.

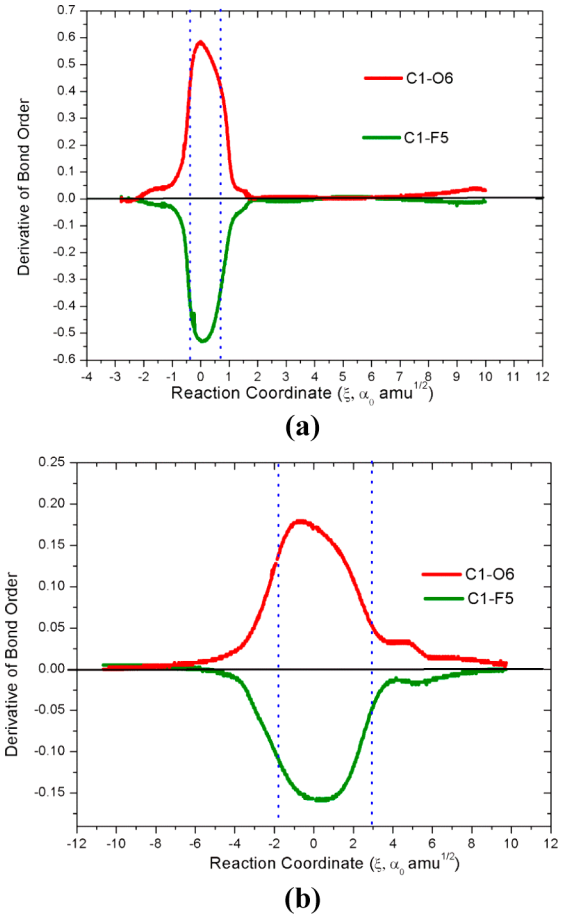

Figure 9. Derivative of Wiberg bond order evolution for a simple S_N2 reaction, viz., $OH^- + CH_3F = CH_3OH + F^-$, in two possible reaction pathways along the reaction coordinate: (a) **path I** and (b) **path II**.

character. It is also interesting to note that the nucleophilic character of OH^- changes to electrophilic at the local minimum (point 4) in **path I**. In this local minimum, F^- center becomes nuclophilic in nature and attacks the electrophilic H center of OH^- to form a hydrogen bonded product. In the case of **path II** the reactivity pattern is quite straightforward. Although in the transition state both OH^- and F^- are nucleophile, the more nucleophilic OH^- attacks to C center of CH_3 to form a similar product as the one from **path I**.

4.4. Comparison with Classical Trajectory. According to Sun et al.,[21] most of the direct dynamics classical trajectory of the S_N2, $OH^- + CH_3F = CH_3OH + F^-$, reaction does not follow the IRC. Very few trajectories follow the IRC, and many trajectories follow the direct dissociation pathway. This means that, rather than forming the H-bonded product, it is producing the product CH_3OH and F^- in such a way that there is no chance to form an H-bonded complex. This happens only if F^- is detached from the CH_3 moiety in a linear fashion. To mimic the trajectory of direct dissociation, we performed a potential energy scan by elongating and decreasing the C−F bond keeping the angle between O−C−F at 180° (It is interesting to note that, if we do not fix the O−C−F angle, a hydrogen-bonded complex will form. Initially, the F^- is going away from the CH_3 moiety in a linear fashion, but after some time, the F^- again comes to the OH moiety to form a stable hydrogen bonded complex. The direct dissociated trajectory can be achieved only when the O−C−F is fixed). We start the potential energy scan from the transition state toward reactant and product. The energy and chemical potential comparison between reaction **paths I** and **III** is given in Figure 12. From the Figure 12, it is evident that the pattern of change of the chemical potential is similar, despite the differences between the energy curves. Although the reaction energy in **path III** is less than in **path I**, we found that the H-bonded product (**path I**) is 20 kcal/mol more stable than the direct dissociated product (**path III**). From the energy profiles, we can say that, although the activation energy for both the reaction **paths I** and **III** is equal, **path I** is thermodynamically favorable.

The difference in energy as a function of reaction coordinate suggests that different reaction mechanisms may be at work along the reaction path. To elucidate this possibility, we now look at the reaction force, reaction electronic flux, separation of reaction electronic flux, NBO, and derivative of Wiberg index analysis. The related associated with **path III** are given in Figure 13. Figure 13 reveals that the force and flux profile of **path III** are similar to **path I** (see Figures 2 and 4). There is a small difference in product region for the force and flux profile. There is a small hump at the product region in **path I** for both the force and flux profile. This is due to the electronic activity that allows the formation of the H-bonded complex. This type of electronic activity is not observed for **path III** as there F is far

dx.doi.org/10.1021/jp3076707 | J. Phys. Chem. A 2012, 116, 10015−10026

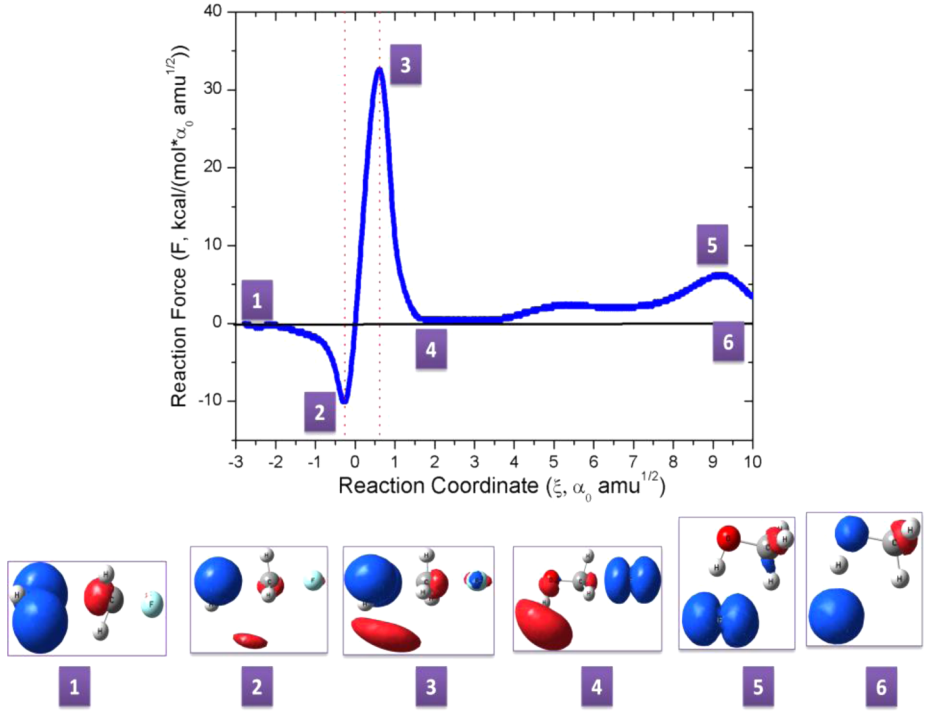

Figure 10. Dual descriptor along the reaction coordinate for a simple S_N2 reaction, viz., $OH^- + CH_3F = CH_3OH + F^-$.

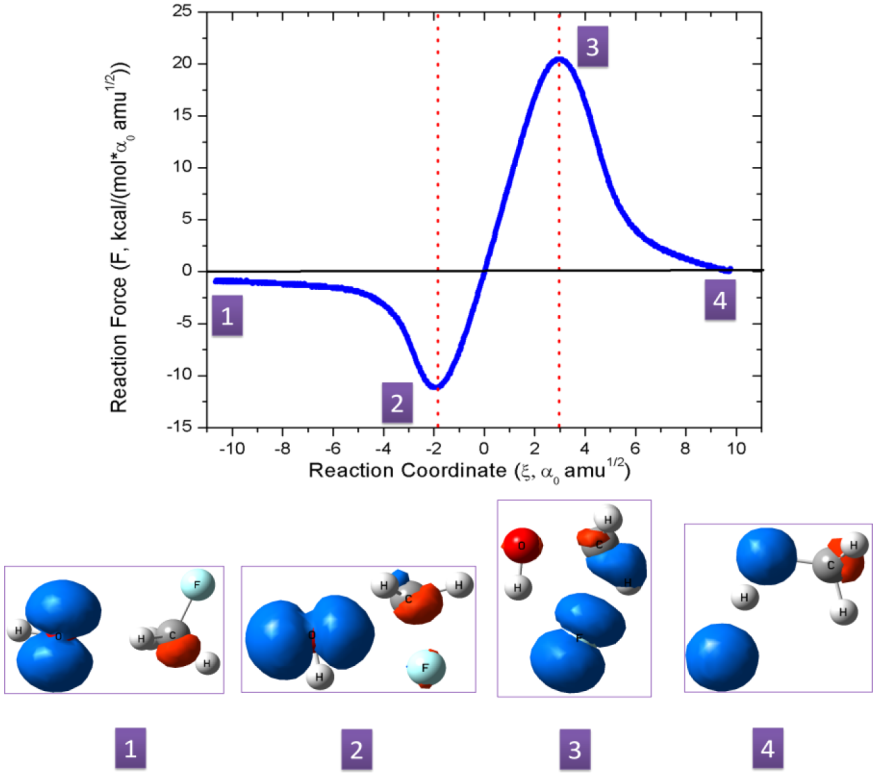

Figure 11. Dual descriptor along the reaction coordinate for a simple S_N2 reaction, viz., $OH^- + CH_3F = CH_3OH + F^-$.

from the CH_3OH moiety. For both reaction paths, flux for electronic transfer is more important than the electronic polarization flux. If we look at the NBO and the derivative of Wiberg index analysis (Figure 13), we also find that both reaction paths almost mimic each other. This means that, during the course of the reaction, the O−C bond is forming and that the C−F bond is breaking to form the desired S_N2 nucleophilic substitution products.

5. CONCLUSIONS

We have throughlly analyzed the mechanism of S_N2 nucleophilic substitution reaction ($OH^- + CH_3F = CH_3OH + F^-$) with the help of reaction force and reaction electronic

dx.doi.org/10.1021/jp3076707 | J. Phys. Chem. A 2012, 116, 10015−10026

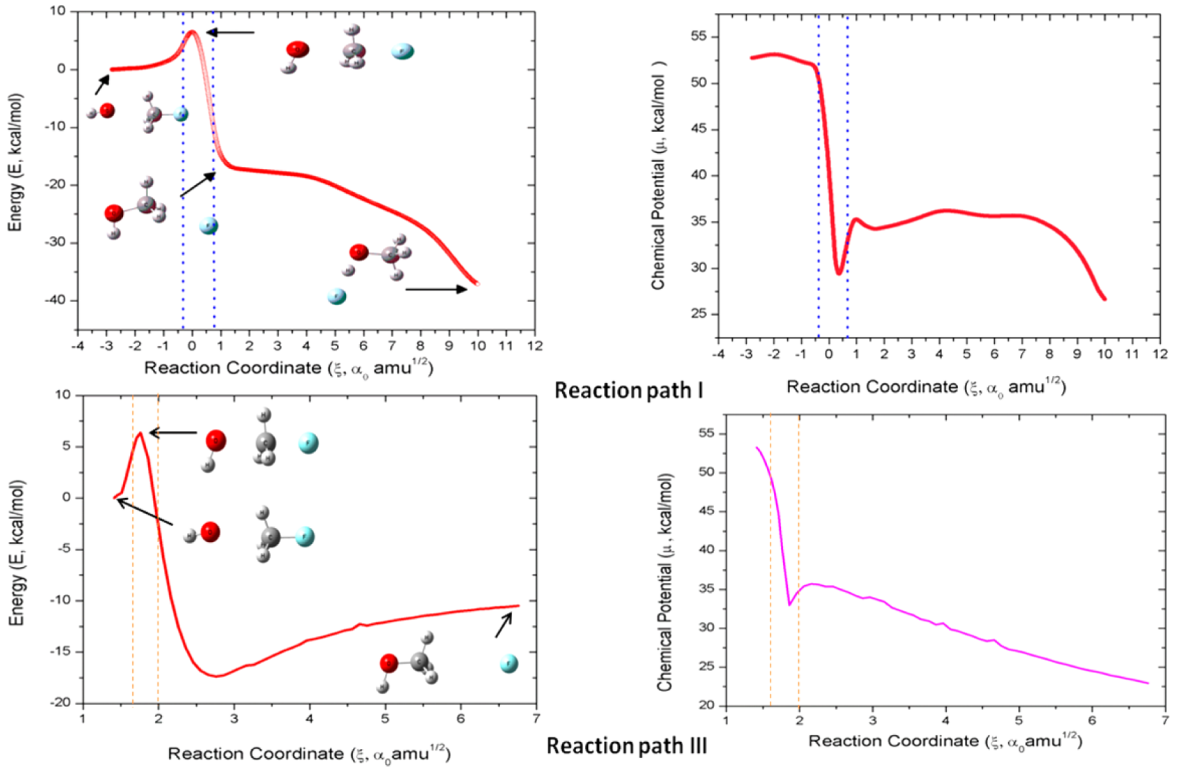

Figure 12. Comparison of energy and chemical potential between reaction **paths I** and **III**.

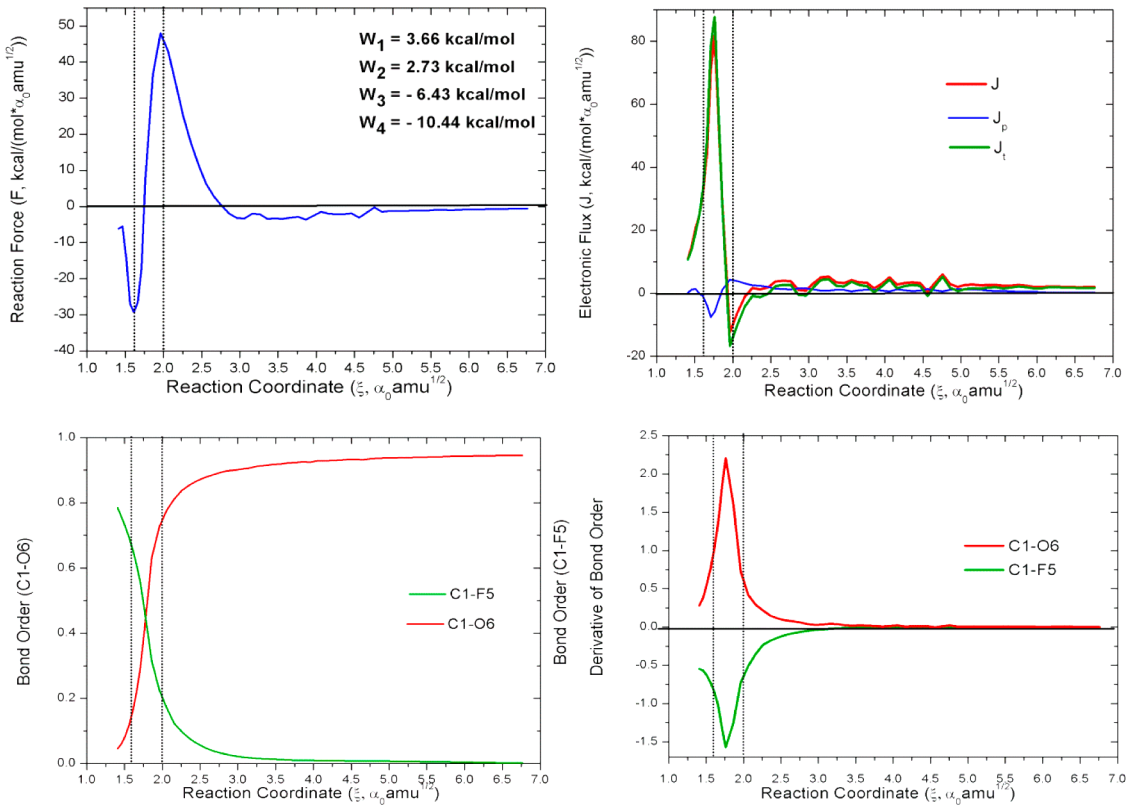

Figure 13. Reaction force, reaction electronic flux, Wiberg index, and derivative of Wiberg index for reaction path **III**.

flux. Two different transition states have been found, which lead to the same product. The electronic transfer component of the reaction flux is the dominant throughout the reaction, but the electronic polarization flux is also significant in the transition state region. To mimic the results from classical trajectory simulation, the direct dissociative product has been formed, but it is 20 kcal/mol less stable than the H-bonded complex. Although the energy profiles are different for **paths I**, **II**, and

dx.doi.org/10.1021/jp3076707 | J. Phys. Chem. A 2012, 116, 10015−10026

III, the chemical driving forces and basic mechanistic details are the same for all three reaction pathways.

AUTHOR INFORMATION

Corresponding Author

*E-mail: atola@puc.cl.

Notes

The authors declare no competing financial interest.

ACKNOWLEDGMENTS

We thank Center for Advanced Interdisciplinary Research in Materials (CIMAT) for financial support. S.G. thanks CIMAT for a postdoctoral fellowship and Laboratorio de Química Teórica Computacional (QTC) for computational facilities. A.T.L. also gratefully acknowledges FONDECYT 1090460 for financial support. P.W.A. thanks NSERC for support.

REFERENCES

(1) Hase, W. *Science* **1994**, *266*, 998.
(2) Bohme, D. K.; Young, L. B. *J. Am. Chem. Soc.* **1970**, *92*, 7354.
(3) Bohme, D. K.; Mackay, G. L.; Payzant, J. D. *J. Am. Chem. Soc.* **1974**, *96*, 4027.
(4) Olmsted, W.; Brauman, J. *J. Am. Chem. Soc.* **1977**, *99*, 4219.
(5) Rossi, R. A.; Pierini, A. B.; Penenory, A. B. *Chem. Rev.* **2003**, *103*, 71.
(6) Ritchie, C. D.; Chappell, G. A. *J. Am. Chem. Soc.* **1970**, *92*, 1819.
(7) Dedieu, A.; Veillard, A. *J. Am. Chem. Soc.* **1972**, *94*, 6730.
(8) Dedieu, A.; Veillard, A. *J. Am. Chem. Soc.* **1973**, *95*, 7715.
(9) Morokuma, K. *J. Am. Chem. Soc.* **1982**, *104*, 3732.
(10) Vande Linde, S. R.; Hase, W. L. *J. Phys. Chem.* **1990**, *94*, 2778.
(11) Ho, M.; Schmider, H. L.; Weaver, D. F.; Smith, V. H.; Sagar, R. P.; Esquivel, R. *Int. J. Quantum Chem.* **1999**, *77*, 376.
(12) Parthiban, S.; Oliveria, G.; Martin, J. M. L. *J. Phys. Chem.* **2001**, *105*, 895.
(13) Gonzales, J.; Pack, C.; Cox, R. S.; Allen, W.; Schaefer, H. F. *Chem.—Eur. J.* **2003**, *9*, 2173.
(14) Gonzales, J.; Allen, W.; Schaefer, H. F. *J. Phys. Chem. A* **2005**, *109*, 10613.
(15) Chattaraj, P. K.; Roy, D. R. *J. Phys. Chem. A* **2006**, *110*, 11401.
(16) Joubert, L.; Pavone, M.; Barone, V.; Adamo, C. *J. Chem. Theory Comput.* **2006**, *2*, 1220.
(17) Chakraborty, D.; Cardenas, C.; Echegaray, E.; Toro-Labbe, A.; Ayers, P. W. *Chem. Phys. Lett.* **2012**, *539*, 168.
(18) Guevara-Garcia, A.; Ayers, P. W.; Jenkins, S.; Kirk, S. A.; Echegaray, E.; Toro-Labbe, A. *Top. Curr. Chem.* **2011**, *128*, 193.
(19) Guevara-Garcia, A.; Echegaray, E.; Toro-Labbe, A.; Jenkins, S.; Kirk, S. A.; Ayers, P. W. *J. Chem. Phys.* **2011**, *134*, 234106.
(20) Toro-Labbé, A. *J. Phys. Chem. A* **1999**, *103*, 4398.
(21) Sun, L.; Song, K.; Hase, W. L. *Science* **2002**, *296*, 875 and references therein.
(22) Parr, R. G.; Yang, W. *Density Functional Theory of Atoms and Molecules*; Oxford University Press: New York, 1997.
(23) Geerlings, P.; De Proft, F.; Langenaeker, W. *Chem. Rev.* **2003**, *103*, 1793.
(24) Johnson, P. A.; Bartolotti, L. J.; Ayers, P. W.; Fievez, T.; Geerlings, P. In *Modern Charge Density Analysis*; Gatti, C.; Macchi, P., Eds.; Springer: New York, 2012; pp 715−764.
(25) Ayers, P. W.; Anderson, J. S. M.; Bartolotti, L. J. *Int. J. Quantum Chem.* **2005**, *101*, 520.
(26) Gazquez, J. L. *J. Mex. Chem. Soc.* **2008**, *52*, 3.
(27) Liu, S. B. *Acta Phys.-Chim. Sin.* **2009**, *25*, 590.
(28) Sen, K. D.; Joegensen, C., Eds. *Structure and Bonding: Electronegativity*; Springer-Verleg: Berlin, Germany, 1987; Vol. *66*.
(29) Parr, R. G.; Donelly, R.; Levy, M.; Palke, W. *J. Chem. Phys.* **1978**, *68*, 3801. Parr, R. G.; Wang, W. *Annu. Rev. Phys. Chem.* **1995**, *46*, 701.
(30) Padmanabhan, J.; Parthasarathi, R.; Subramanian, V.; Chattaraj, P. K. *J. Phys. Chem. A* **2007**, *111*, 1358.
(31) Herrera, B.; Toro-Labbe, A. *J. Phys. Chem. A* **2007**, *111*, 5921.
(32) Ceron, M. L.; Echegaray, E.; Gutierrez-Oliva, S.; Herrera, B.; Toro-Labbe, A. *Sci. China, Ser. B: Chem.* **2011**, *54*, 1982.
(33) Fukui, K. *J. Phys. Chem. A* **1970**, *74*, 4161.
(34) Fukui, K. *Acc. Chem. Res.* **1981**, *14*, 363.
(35) Gonzalez, C.; Schlegel, H. B. *J. Phys. Chem.* **1989**, *90*, 2154.
(36) Hratchian, H. P.; Schlegel, H. B. *J. Chem. Phys.* **2004**, *120*, 9918.
(37) Hratchian, H. P.; Schlegel, H. B. *J. Chem. Theory Comput.* **2005**, *1*, 61.
(38) Herrera, B.; Toro-Labbe, A. *J. Phys. Chem. A* **2004**, *121*, 7096.
(39) Gutierrez-Oliva, S.; Herrera, B.; Toro-Labbé, A.; Chermette, H. *J. Phys. Chem. A* **2005**, *109*, 1748.
(40) Rincon, E.; Jaque, P.; Toro-Labbé, A. *J. Phys. Chem. A* **2006**, *110*, 9478.
(41) Burda, J. V.; Toro-Labbé, A.; Gutierrez-Oliva, S.; Murray, J. S.; Politzer, P. *J. Phys. Chem. A* **2007**, *111*, 2455.
(42) Politzer, P.; Toro-Labbé, A.; Gutierrez-Oliva, S.; Herrera, B.; Jaque, P.; Concha, M. C.; Murray, J. S. *J. Chem. Sci.* **2005**, *117*, 467.
(43) Politzer, P.; Burda, J. V.; Concha, M. C.; Lane, P.; Murray, J. S. *J. Phys. Chem. A* **2006**, *110*, 756.
(44) Rincon, E.; Toro-Labbe, A. *Chem. Phys. Lett.* **2007**, *438*, 93.
(45) Toro-Labbé, A.; Gutierrez-Oliva, S.; Murray, J. S.; Politzer, P. *Mol. Phys.* **2007**, *105*, 2619.
(46) Koopmans, T. *Physica* **1993**, *91*, 651.
(47) Savin, A.; Umrigar, C. J.; Gonze, X. *Chem. Phys. Lett.* **1998**, *288*, 391.
(48) Ayers, P. W.; Morrison, R. C.; Parr, R. G. *Mol. Phys.* **2005**, *103*, 2061.
(49) Ayers, P. W. *J. Math. Chem.* **2008**, *43*, 285.
(50) Cohen, A. J.; Mori-Sanchez, P.; Yang, W. T. *Phys. Rev. B* **2008**, *77*, 115123.
(51) Echagaray, E.; Toro-Labbé, A. *J. Phys. Chem. A* **2008**, *112*, 11801.
(52) Vogt-Geisse, S.; Toro-Labbé, A. *J. Chem. Phys.* **2009**, *130*, 244308.
(53) Flores, P.; Guteirrez-Oliva, S.; Silva, E.; Toro-Labbé, A. *THEOCHEM* **2010**, *943*, 121.
(54) Duarte, F.; Toro-Labbé, A. *J. Phys. Chem. A* **2011**, *115*, 3050.
(55) Cerón, M. L.; Herrera, B.; Araya, P.; Gracia, F.; Toro-Labbé, A. *J. Mol. Model.* **2011**, *17*, 1625.
(56) Boys, S.; Bernardi, F. *Mol. Phys.* **1970**, *19*, 553.
(57) Simon, S.; Duran, M.; Dannenberg, J. *J. Chem. Phys.* **1996**, *105*, 11024.
(58) Sanderson, R. T. *Science* **1955**, *121*, 207.
(59) Sanderson, R. T. *Chemical Bonds and Bond Energy*; Academic Press: New York, 1976.
(60) Parr, R. G.; Yang, W. *J. Am. Chem. Soc.* **1984**, *106*, 4049.
(61) Yang, W.; Mortier, W. *J. Am. Chem. Soc.* **1986**, *108*, 5708.
(62) Yang, W.; Parr, R. G.; Pucci, R. *J. Chem. Phys.* **1984**, *81*, 2862.
(63) Ayers, P. W.; Levy, M. *Theor. Chem. Acc.* **2000**, *103*, 353.
(64) Ayers, P. W. *J. Math. Chem.* **2008**, *43*, 285.
(65) Ayers, P. W.; Yang, W. T.; Bartolotti, L. J. In *Chemical Reactivity Theory: A Density Functional View*; Chattaraj, P. K., Ed.; CRC Press: Boca Raton, FL, 2009; pp 255−267.
(66) Morell, C.; Grand, A.; Toro-Labbe, A. *J. Phys. Chem. A* **2005**, *109*, 1793.
(67) Morell, C.; Grand, A.; Toro-Labbe, A. *Chem. Phys. Lett.* **2006**, *425*, 342.
(68) Morell, C.; Grand, A.; Gutierrez-Oliva, S.; Toro-Labbe, A. In *Theoretical Aspects of Chemical Reactivity*; Elsevier: Amsterdam, The Netherlands, 2007; pp 31−45.
(69) Ayers, P. W.; Morell, C.; De Proft, F.; Geerlings, P. *Chem.—Eur. J.* **2007**, *13*, 8240.
(70) Padmanabhan, J.; Parthasarathi, R.; Elango, M.; Subramanian, V.; Krishnamoorthy, B. S.; Gutierrez-Oliva, S.; Toro-Labbe, A.; Roy, D. R.; Chattaraj, P. K. *J. Phys. Chem. A* **2007**, *111*, 9130.
(71) Becke, A. *J. Chem. Phys.* **1993**, *98*, 5648.
(72) Lee, C.; Yang, W.; Parr, R. G. *Phys. Rev. B* **1988**, *37*, 785.

(73) Reed, A. E.; Curtiss, L. A.; Weinhold, F. *Chem. Rev.* **1988**, *88*, 899.

(74) Frisch, M. J.; Trucks, G. W.; Schlegel, H. B.; Scuseria, G. E.; Robb, M. A.; Cheeseman, J. R.; Scalmani, G.; Barone, V.; Mennucci, B.; Petersson, G. A.; Nakatsuji, H.; Caricato, M.; Li, X.; Hratchian, H. P.; Izmaylov, A. F.; Bloino, J.; Zheng, G.; Sonnenberg, J. L.; Hada, M.; Ehara, M.; Toyota, K.; Fukuda, R.; Hasegawa, J.; Ishida, M.; Nakajima, T.; Honda, Y.; Kitao, O.; Nakai, H.; Vreven, T.; Montgomery, J. A., Jr.; Peralta, J. E.; Ogliaro, F.; Bearpark, M.; Heyd, J. J.; Brothers, E.; Kudin, K. N.; Staroverov, V. N.; Kobayashi, R.; Normand, J.; Raghavachari, K.; Rendell, A.; Burant, J. C.; Iyengar, S. S.; Tomasi, J.; Cossi, M.; Rega, N.; Millam, J. M.; Klene, M.; Knox, J. E.; Cross, J. B.; Bakken, V.; Adamo, C.; Jaramillo, J.; Gomperts, R.; Stratmann, R. E.; Yazyev, O.; Austin, A. J.; Cammi, R.; Pomelli, C.; Ochterski, J. W.; Martin, R. L.; Morokuma, K.; Zakrzewski, V. G.; Voth, G. A.; Salvador, P.; Dannenberg, J. J.; Dapprich, S.; Daniels, A. D.; Farkas, O.; Foresman, J. B.; Ortiz, J. V.; Cioslowski, J.; Fox, D. J. *Gaussian 09*, revision B.01; Gaussian, Inc.: Wallingford, CT, 2009.